

PRACTICAL TOOLS

'Fossils': A new, fast and open-source protocol to simulate muscle-driven biomechanical loading of bone

Narimane Chatar¹  | Romain Boman²  | Valentin Fallon Gaudichon^{1,3} |
Jamie A. MacLaren^{1,4}  | Valentin Fischer¹ 

¹Evolution & Diversity Dynamics lab, UR Geology, Université de Liège, Liège, Belgium

²Department of Aerospace and Mechanical Engineering, Non-Linear Computational Mechanics (MN2L) Research Group, Université de Liège, Liège, Belgium

³Institut des Sciences de l'Evolution de Montpellier (ISEM), Université de Poitiers-Montpellier, Montpellier, France

⁴Functional Morphology Lab, Department of Biology, Universiteit Antwerpen, Antwerpen, Belgium

Correspondence

Narimane Chatar

Email: narimane.chatar@uliege.be

Funding information

Fonds De La Recherche Scientifique - FNRS, Grant/Award Number: 35706165; Fonds pour la Formation à la Recherche dans l'Industrie et dans l'Agriculture, Grant/Award Number: FRIA FC 36251; Fonds Wetenschappelijk Onderzoek, Grant/Award Number: 11Y7615N

Handling Editor: Marta Vidal Garcia

Abstract

1. Finite element analysis (FEA) is a computational method used to predict the behaviour (stresses, strains and deformation) of a structure under predefined loading conditions. It can be applied to different biological structures, such as bone, to study defined muscle-driven scenarios. However, as muscle is an extremely complex structure to model, evolutionary biologists usually model muscle forces indirectly. In 2007, the BONELOAD MATLAB routine was developed to distribute muscle forces on a surface defined by the user. This routine then had to be coupled with a pre-existing FEA software (e.g. Strand7) to perform the analyses and has been widely used ever since.
2. In this manuscript, we present a new method to run muscle-driven finite element simulations on a bone by distributing muscle forces on their insertions area, all within a single environment. We apply this protocol in three different situations: two biting simulations (unilateral and bilateral) and a shoulder flexion simulation.
3. We demonstrate how to prepare the mesh, delineate the muscle origins and insertions, define the constraints, adjust material properties, choose a loading scenario (uniform, tangential or tangential-plus-normal), and extract the results.
4. Our automated script meshes the 3D model, defines the constraints and distributes muscle forces within a single simulation software: 'Metafor' (nonlinear solver, owned and distributed by Gesval S.A) or 'Fossils' (a new open-source linear static solver developed in the frame of this work). 'Metafor' and 'Fossils' can perform the entire protocol (from the meshing to the muscle-induced simulations) on high-resolution volumetric meshes (millions of tetrahedra) and rapidly, exceeding the processing time of other widely used software protocols by up to four times. We demonstrate that the results obtained from our protocol are highly congruent with brands such as Strand7. Thus, our protocol opens up the possibility to routinely and rapidly simulate the behaviour of high-precision muscle-driven FE models containing millions of tetrahedra.

This is an open access article under the terms of the [Creative Commons Attribution-NonCommercial](https://creativecommons.org/licenses/by-nc/4.0/) License, which permits use, distribution and reproduction in any medium, provided the original work is properly cited and is not used for commercial purposes.

© 2022 The Authors. *Methods in Ecology and Evolution* published by John Wiley & Sons Ltd on behalf of British Ecological Society.

KEYWORDS

biomechanics, finite element analysis, muscle loading algorithm, muscle-induced forces, simulation protocol

1 | INTRODUCTION

Finite element analysis (FEA) is a widespread numerical engineering approach used to predict the behaviour (stresses, strains and deformation) of a structure under predefined loading conditions. This modelling approach reduces a complex, three-dimensional (3D) geometry into a finite number of elements with a simpler geometry and predefined properties, size and shape, enabling the quantification of responses by the global geometry to input forces (Zienkiewicz et al., 2005; Zienkiewicz & Morice, 1971). Initially developed in the field of civil engineering, the repeatability, adaptability, non-destructive nature and time-saving benefits of FEA triggered a rapid expansion into medical research (Belytschko et al., 1974; Brekelmans et al., 1972; Coburn, 1980; Huijses & Hollister, 1993; Matthews & West, 1972; Rybicki et al., 1972; Smith & Cohen, 1984). Later, biologists and palaeontologists harnessed the potential of FEA to study the biomechanics of living (and extinct) organisms; since the early 2000s, FEA has grown in its application, becoming the go-to method to analyse biomechanics in human anatomy (Gröning et al., 2012; Joshi et al., 2021), vertebrate feeding (e.g. in sharks Wroe et al., 2008, piranhas Grubich et al., 2012, dinosaurs Rayfield et al., 2001, mammals Tseng, 2009) and locomotion (e.g. in dinosaurs Falkingham et al., 2011, mammals Püschel et al., 2018), and also in invertebrate functional morphology (e.g. Krings et al., 2020).

In palaeontological and comparative studies of animals, the user is often required to model muscles forces indirectly, using punctual forces with origin and focal nodes (Morales-García et al., 2019), or load vectors (Zhou et al., 2019); this overcomes the practical limitation that muscle is an extremely complex structure to model. Few protocols are available to realistically simulate the wrapping of muscle fibres other than the BONELOAD MATLAB routine, initially developed by Grosse et al. (2007), which allows the modelling of muscle-induced forces onto skeletal structures. This script exports Nastran files which can be read by a variety of FEA software, such as Strand7 (Strand7 Pty Ltd). The entire process can therefore be cumbersome, involving multiple software in a strict and repetitive sequence.

Here, we describe and demonstrate a new FEA protocol focusing on the biomechanical analysis of bone (and its mechanical behaviour under muscular load). This protocol is implemented in a new, freely available, open-source linear static solver ('Fossils') and in 'Metafor', a simulation software developed at the University of Liège (Belgium). 'Metafor' has previously been applied to biomechanical questions such as orthodontics (Mengoni et al., 2016), validation tests in subject-specific FE models (Laurent et al., 2016) and applied veterinary orthopaedics (Laurent et al., 2020). We developed a series of routines in 'Fossils' and 'Metafor' to run muscle-driven FE analyses in which three muscle loading scenarios are implemented utilising those already available in the BONELOAD MATLAB routine:

(1) a uniform traction load model, (2) a tangential-traction load model and (3) a tangential-plus-normal-traction load model. We describe the protocol we established to conduct linear static analyses, simulating two different biting scenarios on mandibles (a bilateral bite of an extinct marine reptile, the mosasaurid squamate *Tylosaurus neopaeolicus*; and a unilateral bite of a modern pantherine felid *Panthera pardus*) and a parasagittal shoulder rotation in the Malayan tapir (*Tapirus indicus*). With our protocol, and the open-source linear static solver 'Fossils', we hope to make muscle-driven FEAs available to a larger number of researchers.

2 | MATERIALS

2.1 | Institutional abbreviations

AMNH: American Museum of Natural History (New York, USA), FHSM: Fort Hays Sternberg Museum of Natural History (Hays, USA), NHMW: Naturhistorisches Museum Wien (Vienna, Austria).

3 | PROTOCOL

3.1 | Preparation of the mesh

Surface meshes can be obtained using various methods: photogrammetry, surface scanning (laser or structured light) and CT scanning. The image sequence of the leopard mandible was downloaded from MorphoSource (Media 000009046); image stacks were imported in Avizo lite 2020 (Thermo Fisher Scientific, United States) and the regions of interest were segmented and exported in STL (STereoLithography) format. The mosasaurid mandible was obtained from a Creaform HandyScan 300 laser scanner (0.2mm resolution) and exported as a PLY file from the VX models software (Creaform, United States). The mesh of the tapir scapula and humerus was obtained using a Faro ScanArm Platinum V2 system with integrated Faro Laser Line probe, and exported as PLY files from Geomagic Qualify v.10 (see MacLaren & Nauwelaerts, 2016).

A series of conditions are required to turn a surface mesh composed of triangles into a solid mesh composed of tetrahedra. First, the surface mesh must be completely watertight (consisting of one continuous closed surface) and devoid of non-manifold and self-intersecting faces. A non-manifold geometry can be defined as any edge shared by more than two faces. It is important to note that triangle size and shape (aspect ratio) will influence the quality of the final mesh, and a high aspect ratio will result in a poor quality/low-resolution mesh (see Buser et al. (2020) for more details about steps required to produce a good quality FE mesh). Those steps were performed in Geomagic Wrap 2020

(3D Systems, USA); see ESM for more details on mesh preparation for FEA. Models must be oriented to easily define the constraints along the x, y, z axes; the orientation will depend on the movement studied (see axes drawn of Figure 1). 'Metafor' can call various meshing software (e.g. Tetgen, Gmsh, Samcef) to produce solid meshes; in our example, we called Gmsh (Geuzaine & Remacle (2009) Figure 1). [Correction added on 19 January 2023, after first online publication: Citation to Geuzaine & Remacle added here and to Reference list.] 'Fossils' is internally based on Gmsh for the meshing, calculation and result visualisation; it can thus be considered as an extension to Gmsh. The Gmsh meshing algorithm is quite tolerant with the details of the surface mesh, allowing conversion of surface meshes composed of millions of triangles into solid mesh files. It can handle 'stereolithography' (STL), Wavefront (OBJ) or a 'Polygon File Format' (PLY) (ASCII or binary) files. The path is defined in line 9 relative to the input file as follows:

```
path = os.path.join(os.path.dirname(__file__), '500 k')
```

The surface mesh file is defined in the provided input file for the mosasaurid in line 10 as follows:

```
p['mandible'] = f'{path}/TYLnep_jaw_500k.stl'
```

As an example of triangle-to-tetrahedra conversion, the 500,000 triangles of the mosasaurid surface mesh were converted into a solid mesh with 1,996,413 tetrahedra.

3.2 | Muscle delineation and constraints definition

Parts of the surface meshes representing muscle insertions and origins must be selected directly on the meshes; if analyses at different resolutions are required, then muscles have to be drawn on every surface mesh so that they fit with the corresponding mesh. Each selection of facets corresponding to muscle insertion on the structure of interest should be exported as a separate STL, OBJ or PLY file (one surface mesh per muscle insertion). Only faces representing the attachment area have to be exported. Muscle origins on the connected bones should also be drawn to assess the centroid of the origin, which defines the point towards which the traction will be applied. In our examples, the jaws were articulated with the cranium to define the origin and muscle paths for the biting scenarios, and the scapula was articulated with the humerus to define origin and muscle paths for the shoulder flexion scenario. Any software capable of creating a 3D object based on a selection, and to estimate the geometric centroid of an object surface, could be used for these steps. Figure S2 shows an example of muscle surface delineation with our three specimens, using Geomagic Wrap 2020 (3D Systems, United States) for the leopard and the mosasaurid, and using Blender (Blender Foundation, The Netherlands) for the tapir.

Boundary conditions must now be defined, which will depend on the scenario being tested. Boundary conditions are defined as xyz coordinates of precise surface nodes. In the given examples, the leopard model was constrained by three degrees of freedom (xyz) on the biting point, and we allowed lateral translation at both jaw articulations (temporomandibular joints; TMJs), constrained in y- and z-axes only (see Figure 1 for a graphical representation of the constraints); the mosasaurid mandible boundary conditions were

constrained by three degrees of freedom (no xyz translations) at the jaw articulation (quadratmandibular joint), and by one degree of freedom (z, dorsoventral axis only) at the biting point. The two constraint points at the jaw articulation joints were defined in lines 13 and 14 of the input file: for example, for the mosasaurid mandible.

```
p['axis_pt1'] = [381.261627, 39.182289, 82.731766]
```

```
p['axis_pt2'] = [391.689667, 381.874176, 81.844215]
```

For a unilateral bite such as in our example of the leopard mandible, one single biting point was defined line 11 of the input file:

```
p['contact_pts'] = [16.4418, 17.3567, -53.2842]
```

In our example of a bilateral bite, the mosasaurid mandible required two biting points to be defined in lines 11 and 12 of the input file:

```
p['contact_pts'] = [[-417.999359, 222.242569, 31.007950],
[-428.224182, 162.031265, 36.896519]]
```

For the tapir shoulder, we defined three points: two on the humeral head to model the articulation with the scapula, and one on the most distal point of the humeral trochlea. It is important that the articulation is defined by two points to create a rotation axis, limit the freedom, and maintain an isostatic system (Figure S3). While this is evident for our biting simulations, since there are two articulation points with the cranium (left and right sides), this also had to be modelled for our shoulder simulation (generating a parasagittal flexion scenario).

Coordinates of the constraint points can be obtained using any software capable of extracting coordinates of precise points; examples include Meshlab or Geomagic. The degrees of freedom should then be adjusted (lines 89–92 of the script):

```
p['fixations'] = {
'contact_pts': ['z'],
'axis_pt1': ['x';'z','y'],
'axis_pt2': ['x';'z','y']
}
```

3.3 | Material properties

The constitutive law for the bone (the stress–strain relationship) is simplified to a homogeneous isotropic linear elastic behaviour which requires three parameters: bone density (more precisely, the specific mass) (T/mm^3), Young's modulus (MPa) and Poisson's ratio. The material properties for the leopard were set as 18,000 MPa for the Young's modulus, 0.3 for the Poisson ratio (Currey, 1987; Currey & Brear, 1990; Erickson et al., 2002) and $1.662e-9 T/mm^3$ for the density; these are defined in the input file in lines 60–62 of the input file:

```
# material properties
p['density'] = 1.662e-9 #[T/mm3]
p['Young'] = 18000. #[MPa]
p['Poisson'] = 0.3 #[-]
```

The density is not theoretically required for linear static simulations, but as 'Metafor' is a dynamic implicit nonlinear solver we needed to define a density value to perform a single time increment.

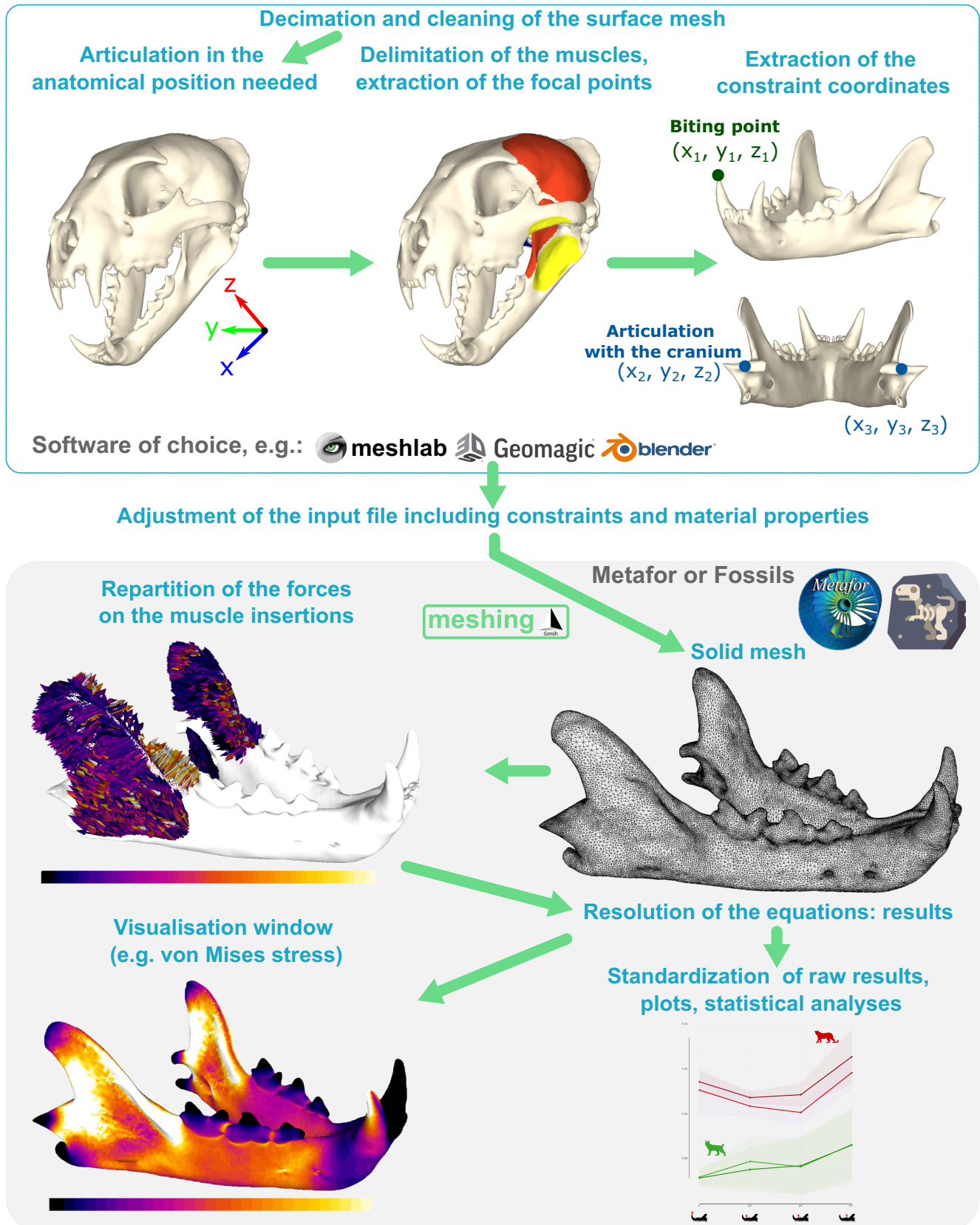


FIGURE 1 Complete workflow of the ‘fossils’ protocol, shown on a leopard mandible (*Panthera pardus* AMNH-113745). Steps in the top box can be done with a 3D processing software of choice (e.g. Meshlab, Geomagic, Blender); steps in the lower box are performed in ‘Fossils’ or Metafor. See ESM and Figure S1 for the workflow shown on the three examples. Bottom right: Example of results from Chatar, Fischer, and Tseng (2022).

This increment is large enough (1 s) to avoid any dynamic effects in the results. For our mosasaurid mandible example, material properties were set as 15,000 MPa for the Young's modulus (e.g. Foffa et al., 2014; Zapata et al., 2010), bone density was set to $1.662 \times 10^{-9} \text{ T/mm}^3$ (e.g. Porro et al., 2011, 2013; Zapata et al., 2010) and the Poisson's ratio was set to 0.3, in accordance with Currey (1987), Currey and Brear (1990), and Erickson et al. (2002) (see input file lines 96 to 98).

3.4 | Loading

The STL files of each muscle insertion should now be called in the muscle list:

```
p['muscles'] = [
{
'file': f'{path}/M_AE_L1.stl',
'force': 2237.69,
'focalpt': [281.827445, 30.054466, 237.947288],
'method': 'T+N' # 'U', 'T', 'T+N'
},
```

A dictionary is created for each muscle group containing the STL file (e.g. for the *m. adductor externus* on the mosasaurid mandible: 'file': f'{path}/M_AE_L1STL'); the force to be applied on this precise insertion (e.g. 'force': 2237.69), the xyz coordinates of the

centroid of the muscle origin on the corresponding structure (in our case the cranium, e.g. for the *m. adductor externus*: 'focalpt': [281.827445, 30.054466, 237.947288], and finally the loading scenario ('method'). Loading scenarios implementable in 'Metafor' and 'Fossils' can be defined to a uniform traction load model 'U', a tangential-traction load model 'T', and a tangential-plus-normal-traction load model 'T+N'. Figure 2 shows the repartition of forces on the 3D model of a cylinder under these different loading scenarios.

In the uniform scenario (U), the force vectors go through the surface of the bone (Figure 2a); the tangential traction scenario (T) simulates the wrapping of the muscle fibres around the bone (Figure 2b); the tangential-plus-normal-traction scenario (T+N) adds the normal of the force pulling on the bone (Figure 2c). The tangential-plus-normal-traction load model represents the most accurate, life-like model, and the computation time remains reasonable, for example, <30 min to mesh and analyse the mosasaurid mandible (500k triangles). Those three traction models were the three scenarios initially implemented in BONELOAD by Grosse et al. (2007), and although the uniform traction is available for users, it is far from realistic. The use of load vectors might be more accurate than loading the bone using a uniform traction, but we posit that this also depends on the bone architecture and the position/inclination of the muscle origins and insertions. The python

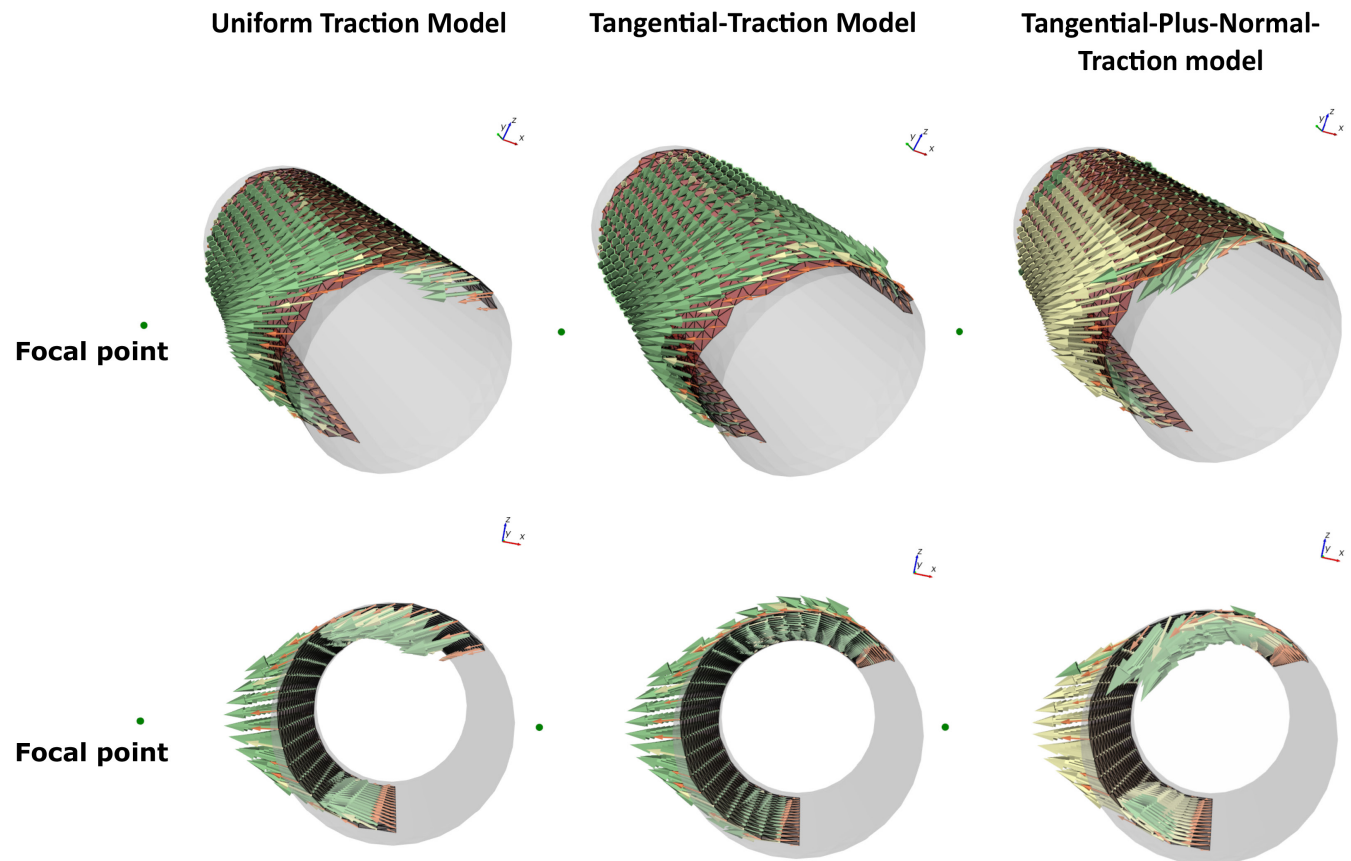


FIGURE 2 Comparison of traction models implemented in the input script of the 3D model of a cylinder representing a bone. The cylinder represents a bone, the red surface a muscle insertion, the green arrows are the forces and the focal point is the centre of mass of the muscle origin.

script 'loadbone.py' is based on the BONELOAD routine initially published by Grosse et al. (2007). However, some changes were made to the BONELOAD routine to adjust the pressure magnitude and increase efficiency. In the simplest model—the Uniform-Traction model—the total traction force \bar{F} applied by a muscle on the bone is uniformly distributed on the surface mesh of the muscle attachment. For each triangle of this mesh, the traction is assumed to be directed towards a focal node modelling the opposite muscle attachment (see Figure 3a).

If o is the focal node, the force direction d^i related to the i th triangle corresponds to the unit vector in Equation 1.

$$d^i = \frac{o - c^i}{\|o - c^i\|} \quad (i = 1, 2, \dots, n_{tri}), \quad (1)$$

where n_{tri} is the total number of triangles and c^i is the barycentre of triangle i .

In Equation 2, the nodal force corresponding to a unit traction d^i acting on the j th node of the i th triangle is then computed as

$$f_j^i = \frac{A_i}{3} d^i \quad (j = 1, 2, 3), \quad (2)$$

where A_i is the area of triangle i .

The forces of all the individual triangles are then assembled into a structural vector F^* (Equation 3), whose components are the sum of the contributions of the neighbouring triangles of each node:

$$F^* = \sum_{ij} f_j^i. \quad (3)$$

Eventually, this load vector is scaled so that its magnitude corresponds to the prescribed value \bar{F} (Equation 4).

$$F = \bar{F} \frac{F^*}{\|F^*\|}. \quad (4)$$

The two other methods follow the same procedure, except that the direction d^i is computed in a more realistic way. If a triangle does not have a direct line of sight to the focal point (Figure 3b, right), the direction calculated by the latter method gives a compressive force towards the interior of the bone, although the muscle fibres wrap around the surface of the bone. The forces should therefore be mainly oriented along a tangent to the surface. This drawback of the uniform-traction model leads to a refinement in the second model of force distribution—the Tangential-Traction model—which is implemented as follows. Let us define n , the outward unit normal to a given triangle of the surface mesh. If

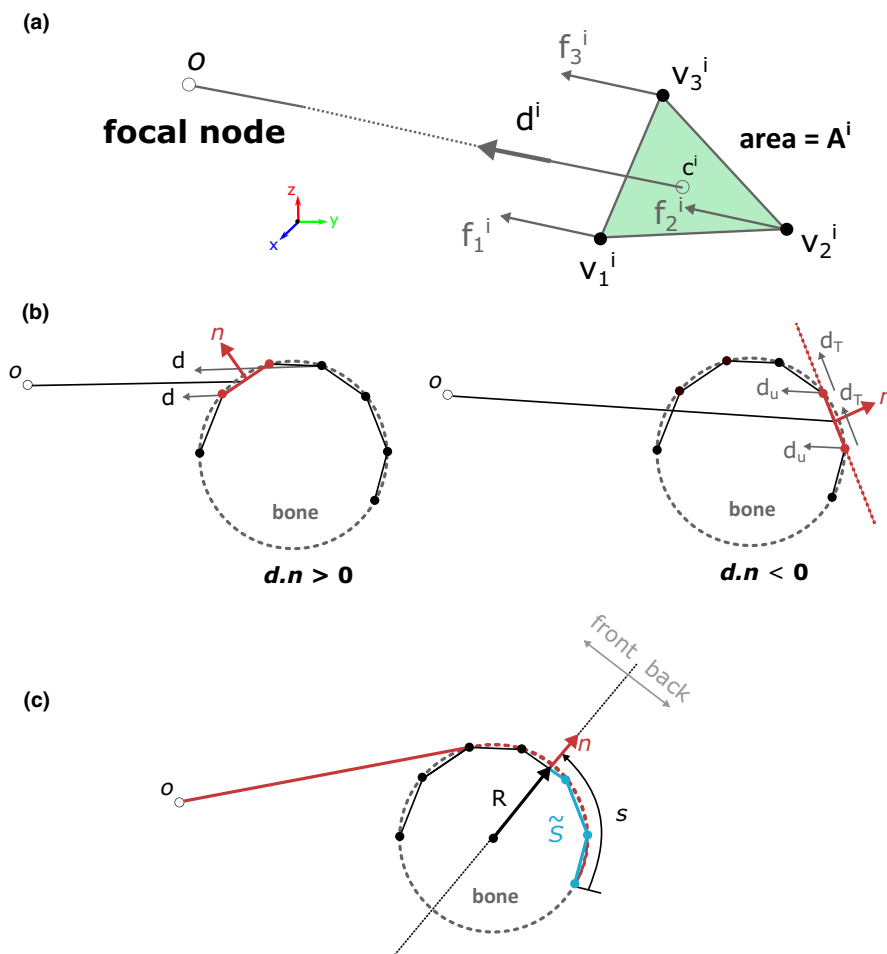


FIGURE 3 (a) Computation of the nodal forces acting on a triangle of the surface mesh of a muscle group. In the uniform-traction model, the forces are aligned towards the force focal node o representing the opposite muscle attachment. (b) Projection of the force direction d_U when the triangle does not have a direct line of sight to the focal point. The new direction d_T is tangent to the surface mesh in the plane defined by the focal point o and the normal vector n . (c) Calculation of the approximation s of fibre length s from the origin of the muscle fibre bundle to the centre of the current triangle and the local radius R of curvature at the same point. These two lengths must be measured in the plane defined by the focal point o and the normal vector n .

$d \cdot n > 0$ (as in Figure 3b, left), the previous direction d^i is kept and the forces acting on the triangle are the same as before. However, if $d \cdot n < 0$ (Figure 2, right), the direction is projected onto the plane of the triangle and normalised again. The corrected direction d_T (Equation 5) becomes:

$$d_T = \frac{d_U - (d_U \cdot n) n}{\|d_U - (d_U \cdot n) n\|}, \quad (5)$$

where d_U is the direction computed as in the Uniform-Traction model. The new direction d_T is much more realistic and is not expensive in

terms of additional calculations. Note that the index i will be omitted in the following expressions to simplify the notations.

The third model—the Tangent-Plus-Normal model—is similar to the Tangential-Traction method but adds a normal component to the tangential contribution which models the compressive action of the muscle fibres that wrap around the bone on top of each other. This additional pressure acts only if the surface is locally convex, and its amplitude is proportional to the length s of the muscle fibre bundle in the plane defined by the focal point o and the normal vector n as depicted in Figure 3. The new direction d_{T+N} (Equation 6) including both tangential and normal components is evaluated as

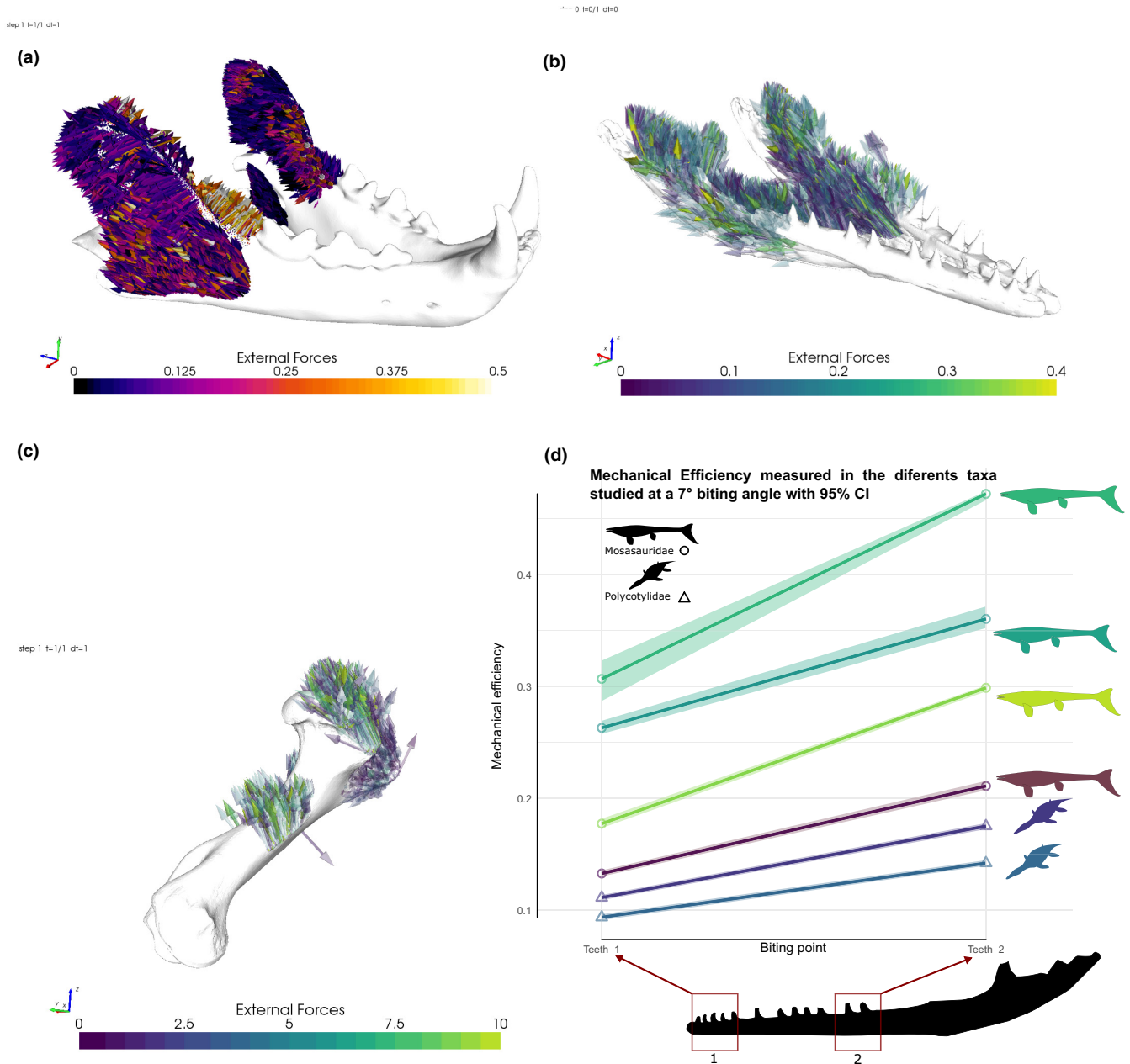


FIGURE 4 Traction vectors on (a) the leopard mandible, (b) the mosasaurid mandible, (c) on the tapir humerus, showing the distribution of forces on the muscle insertions. (d) Example of plot to illustrate some of the results which can be extracted from the analyses. Here, the mechanical efficiency (reaction force divided by the total input force) at two different biting points in different marine reptiles is shown, results from Fallon Gaudichon et al. (2021).

$$\mathbf{d}_{T+N} = \mathbf{d}_T + \frac{\mathbf{s}}{R} \mathbf{n} \quad \text{when } R < 0, \quad (6)$$

where R is the local radius of curvature in the plane defined by \mathbf{o} and \mathbf{n} . Note that \mathbf{d}_{T+N} is not a unit vector anymore.

Contrary to the Tangential-Traction model, the evaluation of this expression is extremely costly since it requires cutting the surface mesh by a plane. The cutting operation has been implemented with the help of the VTK library, which is commonly used for displaying meshes on computer screens. VTK also comes with a series of very robust algorithms for modifying and manipulating meshes. These algorithms are very efficient since they target real-time visualisation. For each triangle, the surface mesh of the muscle attachment is first cut by a plane normal to \mathbf{d}_T and passing through the barycentre \mathbf{c} of the triangle. This operation divides the mesh into a front and a back part (see Figure 3) which are needed to identify the part containing the origin of the fibre bundle. Next, the intersection of both parts with the plane defined by \mathbf{o} and \mathbf{n} is calculated. The result of this operation is two sets of piecewise linear segments, which correspond to the mesh displayed in Figure 3c. The vertices are sorted and the fibre length s is approximated by \tilde{s} , the sum of the lengths of the line segments coming from the back part of the surface mesh (the blue segments in Figure 3c). Then, a smooth high-order polynomial approximation $p(t)$ of the bone surface shape is built in the local axes $(\mathbf{d}_T, \mathbf{n})$ from the position of the first two vertices found on both sides of the current triangle. The curvature of this polynomial at the barycentre \mathbf{c} of the triangle can be easily calculated by Equation 7.

$$\frac{1}{R} = \frac{p''(0)}{(1+p'(0)^2)^{3/2}}, \quad (7)$$

where p' and p'' denote the first and second derivatives of $p(t)$.

Once the \mathbf{d}_{T+N} vectors have been calculated for every triangle of the muscle attachment surface, they are assembled and scaled as in the Uniform-Traction model. Thanks to VTK, the total CPU time required to create this much more realistic distribution of muscle-driven forces remains reasonable, even for very fine meshes (a few seconds). A visual representation of the force repartition on the muscle insertions can be seen in Figure 4.

A step-by-step guide explaining how to launch 'Metafor' and extract the results is available in the ESM. 'Fossils' will simply open a Gmsh window for the results visualisation when calculations are complete, and creates a log file (stdout.txt) that include the results. 'Fossils' writes the resulting nodal forces in a simple format (a table with four columns: node#, fx, fy, fz), which can be easily extracted and translated into another format.

The current protocol does not allow users to work with multiple material properties. However, this is possible with the use of 'geniso', a tool developed in 'Metafor' (see D'Ottreppe et al., 2012), which automatically generates multi-material meshes from data segmented using 3D Slicer (<https://www.slicer.org/>). This would require skipping the first steps (decimation, cleaning and preparation of the mesh) and directly providing the solid mesh to 'Metafor' or 'Fossils'.

4 | COMPARISON WITH OTHER PROTOCOLS

We ran the same analysis on our three examples using 'Metafor', 'Fossils' and the widely used MATLAB/Strand7 to compare the meshing and model resolution times and the results obtained (see Table 1). Analyses in 'Metafor' and 'Fossils' were performed using an ASUS laptop Intel Core i5 -8300H, 2.30GHz Quad Cores with 32GB of RAM, whereas analyses in Strand7 were performed on a workstation Intel Xeon Silver 4208, 2.10Ghz Octa Core with 64GB of RAM. To compare the different software on equal terms, we did not run the analyses in parallel as the Strand7 R2 version we used did not allow it (both 'Metafor' and 'Fossils' could handle parallel processing).

Here we detail the durations obtained for the leopard mandible, the mosasaurid mandible and the tapir shoulder (detailed in Tables 1 and 2 and Figure 5).

Strand7 took 17m 16s to turn the 199,804 triangles mesh into a 1,004,460 tetrahedra mesh; creating the Nastran files and the MS Excel template to run the BONELOAD MATLAB routine took 5m 32s; distributing the forces on the muscle insertions using a tangential-plus-normal traction model took 12m 19s; Strand7 solved the equation in 5m 57s; thus, the entire process took a minimum duration of 41m 4s.

Our 'Metafor' protocol is four times faster: the creation of the solid mesh (from the same initial surface mesh, resulting in 797,466

TABLE 1 Comparison of durations for different steps in the finite element analysis (FEA) protocols compared. Note that for the mosasaurid mandible, the model had to be decimated to 250k triangles to use the Strand7 meshing algorithm, and BONELOAD was unable to apply a tangential-plus-normal traction in this particular case so the tangential traction was applied instead. Note also that the time presented in this table does not include the delineation of muscle groups and the definition of constraints, which (while time-consuming) is considered a uniform duration as all protocols utilise the same muscle group delineations/constraints

	Meshing	Forces distribution	Resolution	Total
<i>Panthera pardus</i> Initial number of triangles in the surface mesh: 200k				
Metafor	6 m 24s		3 m 28s	9 m 52s
Strand7	17m 16s	12 m 19s	5 m 32s	41m 4 s
Fossils	6 m 16s		1 m 53s	8 m 9 s
<i>Tapirus indicus</i> Initial number of triangles in the surface mesh: 50k				
Metafor	1 m 9 s		1 m 11 s	2 m 20s
Strand7	1 m 40s	1 m 22s	2 m 12s	5 m 14s
Fossils	50s		1 m 23s	2 m 03s
<i>Tylosaurus nepaeolicus</i> Initial number of triangles in the surface mesh: 500k (250k for Strand7)				
Metafor	7 m 2 s		24m 14s	31m 16s
Strand7	27m 43s	2 m 53s	5 m 19s	35m 55s
Fossils	6 m 43s		9 m 53s	15m 36s

TABLE 2 Comparison of outputs for the same finite element analysis in 'Metafor', Strand7 and 'Fossils'

	Number of tetrahedra	Reaction force (N)	Internal energy (mJ)	Max displacement (mm)
<i>Panthera pardus</i> Initial number of triangles in the surface mesh: 200k				
Metafor	797,46	157.62	171.93	2.08
Strand7	1,004,460	157.62	196.52	2.59
Fossils	797,466	154.54	171.18	2.14
<i>Tapirus indicus</i> Initial number of triangles in the surface mesh: 50k				
Metafor	226,076	3334.07	13,012.60	3.37
Strand7	243,522	4562.61	7258.89	3.55
Fossils	226,076	3323.17	12,410.97	3.22
<i>Tylosaurus nepaeolicus</i> Initial number of triangles in the surface mesh: 500k (250k for Strand7)				
Metafor	1,996,413	3971.70	116,072.00	56.69
Strand7	1,512,889	4397.67	87,327.11	52.44
Fossils	1,996,413	3927.28	74,234.67	54.71

tetrahedral elements) and the distribution of forces totalled 6 m 24s, and equation solving amounted to 3 m 28s; the total protocol thus took 'Metafor' 9 m 52s. 'Fossils' was even faster, as the meshing and forces distribution combined took 6 m 16s and the model resolution took 1 m 53s, for a total of 8 m 9 s (Figure S6). In addition, to be able to mesh the mosasaurid mandible in Strand7, the surface mesh had to be decimated to 250k triangles, whereas both 'Metafor' and 'Fossils' had no problems in meshing the 500k triangles model. Moreover, we could not use BONELOAD to apply a tangential-plus-normal traction in this particular case, so tangential traction was applied instead. The reaction forces (measured on the biting tooth) and maximum displacement were similar, as was the resultant internal energy (Table 2); the von Mises stress contour plots are also strongly congruent (Figure 5). Results of the biting simulations for the leopard mandible were nearly identical, with the exact same reaction forces (to two decimal places) recovered by 'Metafor' and Strand7, and only 0.43% of variation in terms of internal energy (Table 2). The shoulder rotation in the

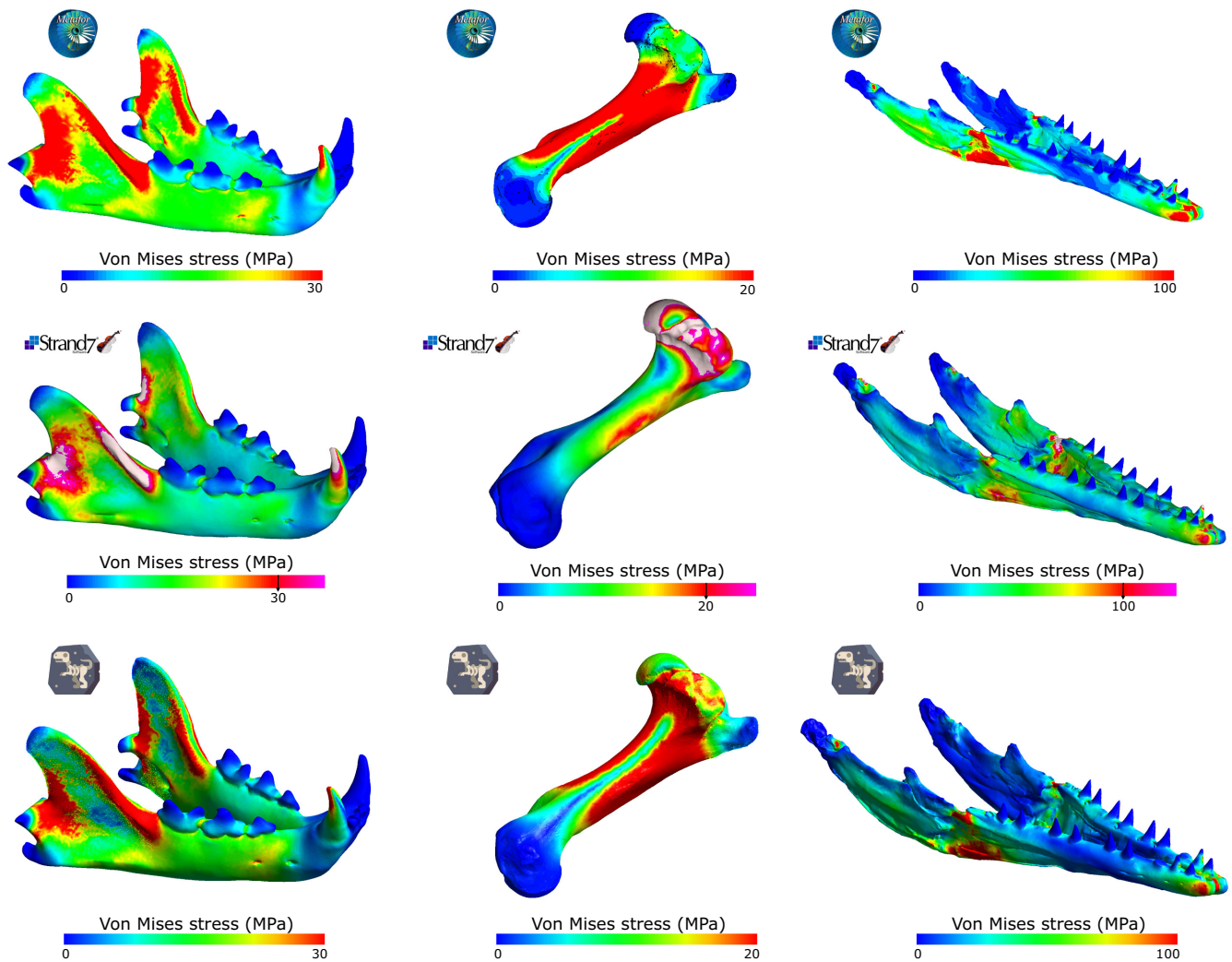


FIGURE 5 Comparison of von Mises stress contour plots obtained using 'Metafor' (top), Strand7 (middle) and 'Fossils' (bottom). The 'default' and 'rainbow' colour palettes were used in 'Metafor', 'Fossils' and Strand7, respectively, as the choice of colour palette in Strand7 is limited.

tapir was the most complex scenario modelled, but also yielded similar values in terms of reaction force, internal energy and maximum displacement; however, the von Mises stress distributions appear more variable than in the other scenarios. Although the results obtained with 'Metafor' and 'Fossils' are always similar when dealing with small displacements (leopard and tapir simulations), they differ substantially when larger displacements are computed (e.g. the mosasaurid simulation), because the hypothesis of small displacements made in 'Fossils' is violated. Still, the overall stress distribution in the mosasaurid biting simulation was consistent across the three finite element codes compared, demonstrating that 'Metafor' and 'Fossils' are two fast and valid alternatives.

5 | CONCLUSIONS

We present a new protocol to simulate biomechanical loading of bone. Our protocol automatically combines meshing, definition of constraints, analysis and visualisation of muscle forces in a single simulation tool, freely available for academic purposes ('Metafor'), and we introduce a new freely open-source solver: 'Fossils'. Using the VTK library for geometric calculations shortens the processing time compared to other similar protocols, allowing muscle-induced biomechanical simulations on skeletal structures using high-resolution 3D models (i.e. containing millions of tetrahedra). These solutions can be performed in a relatively short amount of time, resolving models four times faster than other leading finite element modelling software (e.g. Strand7 + MATLAB combo), all-the-while yielding very similar results. We apply our protocol on vertebrate mandibles and long bones in biting and rotation scenarios, respectively, to demonstrate the flexibility of the protocol.

AUTHOR CONTRIBUTIONS

Narimane Chatar, Romain Boman and Valentin Fischer designed the project. Romain Boman implemented the 'Fossils' solver and the python version of BONELOAD. Narimane Chatar, Valentin Fallon Gaudichon, Jamie A. MacLaren collected raw data and ran the analyses. Narimane Chatar and Romain Boman wrote the initial draft. All authors contributed to subsequent drafts and approved the final manuscript.

ACKNOWLEDGEMENTS

Authors would like to thank Prof. Z. Jack Tseng (FAVE Lab, UC Berkeley) for his help, time and dedication in explaining the BONELOAD MATLAB routine and FEA in general. NC is grateful to the whole FAVE Lab for access to the workstation that allowed comparisons with Strand7. NC is supported by a grant of Fonds de la Recherche Scientifique F.R.S.-FNRS (FRIA grant number FRIA FC 36251); additional funding for specimen acquisition was provided by a F.R.S.-FNRS travel grant (35706165) and FWO Doctoral Fellowship (11Y7615N), both awarded to JAM. Finally, we thank the MEE editorial board, as well as Dr. Stephan Lautenschlager and four

anonymous reviewers for their constructive comments on a previous version of the manuscript.

CONFLICT OF INTEREST

We declare we have no competing interests.

PEER REVIEW

The peer review history for this article is available at <https://www.webofscience.com/api/gateway/wos/peer-review/10.1111/2041-210X.14051>.

DATA AVAILABILITY STATEMENT

'Metafor' is owned and distributed by Gesval S.A., a public limited company created by the University of Liège to manage its intellectual property. Installation files and academic licences are available upon request for research purposes only; to obtain an installation file and a licence please contact Romain Boman (r.boman@uliege.be).

The source code of 'Fossils', all the input files and the 'Metafor' scripts are available in the [Supplementary Material](#), on the GitLab server of the University of Liège (<https://gitlab.uliege.be/R.Boman/fossils>), and on Zenodo (Chatar, Boman, et al. (2022), <https://doi.org/10.5281/zenodo.6719190>).

Boneload python script to run muscle induced analyses in 'Metafor': <https://gitlab.uliege.be/R.Boman/fossils/-/tree/master/models/boneload.py>

Bone model python script: <https://gitlab.uliege.be/R.Boman/fossils/-/tree/master/models/bonemodel.py>.

Examples presented in the manuscript: *Tylosaurus nepaeolicus* FHSM-VP-2209: <https://gitlab.uliege.be/R.Boman/fossils/-/tree/master/models/TYLnep>.

Panthera pardus AMNH-113745 https://gitlab.uliege.be/R.Boman/fossils/-/tree/master/models/Panthera_pardus.

Tapirus indicus NHMW 1938: https://gitlab.uliege.be/R.Boman/fossils/-/tree/master/models/Tapirus_indicus.

Strand7 files used for comparison: <https://gitlab.uliege.be/rboman/fossils/-/tree/master/strand7>.

Tutorial showing how to instal 'Metafor': <http://metafor.ltas.ulg.ac.be/dokuwiki/doc/user/tutorials/installation>.

ORCID

Narimane Chatar  <https://orcid.org/0000-0003-0449-8574>

Romain Boman  <https://orcid.org/0000-0002-4883-0383>

Jamie A. MacLaren  <https://orcid.org/0000-0003-4177-227X>

Valentin Fischer  <https://orcid.org/0000-0002-8808-6747>

REFERENCES

- Belytschko, T., Kulak, R. F., Schultz, A. B., & Galante, J. O. (1974). Finite element stress analysis of an intervertebral disc. *Journal of Biomechanics*, 7(3), 277–285. [https://doi.org/10.1016/0021-9290\(74\)90019-0](https://doi.org/10.1016/0021-9290(74)90019-0)
- Brekelmans, W. A. M., Poort, H. W., & Slooff, T. J. J. H. (1972). A new method to analyse the mechanical behaviour of skeletal parts. *Acta Orthopaedica*, 43(5), 301–317. <https://doi.org/10.3109/17453677208998949>

- Buser, T. J., Boyd, O. F., Cortes, A., Donatelli, C. M., Kolmann, M. A., Luparell, J. L., Pfeiffenberger, J. A., Sidlauskas, B. L., & Summers, A. P. (2020). The natural Historian's guide to the CT galaxy: Step-by-step instructions for preparing and analyzing computed tomographic (CT) data using cross-platform, open access software. *Integrative Organismal Biology*, 2(1), obaa009. <https://doi.org/10.1093/IOB/OBAA009>
- Chatar, N., Boman, R., Gaudichon, V., MacLaren, J., & Fischer, V. (2022). A new, fast protocol to simulate biomechanical loading of bone (1.0). Zenodo. <https://doi.org/10.5281/zenodo.6719190>
- Chatar, N., Fischer, V., & Tseng, Z. J. (2022). Many-to-one function of cat-like mandibles highlights a continuum of sabre-tooth adaptations. *Proceedings of the Royal Society B: Biological Sciences*, 289(1988), 20221627. <https://doi.org/10.1098/rspb.2022.1627>
- Coburn, B. (1980). Electrical stimulation of the spinal cord: Two-dimensional finite element analysis with particular reference to epidural electrodes. *Medical & Biological Engineering & Computing*, 18(5), 573–584. <https://doi.org/10.1007/BF02443129>
- Currey, J. D. (1987). The evolution of the mechanical properties of amniote bone. *Journal of Biomechanics*, 20(11–12), 1035–1044. [https://doi.org/10.1016/0021-9290\(87\)90021-2](https://doi.org/10.1016/0021-9290(87)90021-2)
- Currey, J. D., & Brear, K. (1990). Hardness, Young's modulus and yield stress in mammalian mineralized tissues. *Journal of Materials Science: Materials in Medicine*, 1(1), 14–20. <https://doi.org/10.1007/BF00705348>
- D'Ottreppe, V., Boman, R., & Ponthot, J.-P. (2012). Generating smooth surface meshes from multi-region medical images. *International Journal for Numerical Methods in Biomedical Engineering*, 28, 642–660. <https://doi.org/10.1002/cnm.1471>
- Erickson, G. M., Catanese, J., & Keaveny, T. M. (2002). Evolution of the biomechanical material properties of the femur. *Anatomical Record*, 268(2), 115–124. <https://doi.org/10.1002/ar.10145>
- Falkingham, P. L., Bates, K. T., Margetts, L., & Manning, P. L. (2011). Simulating sauropod Manus-only trackway formation using finite-element analysis. *Biology Letters*, 7(1), 142–145. <https://doi.org/10.1098/RSBL.2010.0403>
- Fallon Gaudichon, V., Boman, R., Chatar, N., Maclaren, J., & Fischer, V. (2021, September). Uncovering the biomechanical disparity of cretaceous marine reptile feeding via finite element analysis. 69th symposium on vertebrate palaeontology and comparative anatomy.
- Foffa, D., Cuff, A. R., Sassoon, J., Rayfield, E. J., Mavrogordato, M. N., & Benton, M. J. (2014). Functional anatomy and feeding biomechanics of a giant Upper Jurassic plesiosaur (Reptilia: Sauropterygia) from Weymouth Bay, Dorset, UK. *Journal of Anatomy*, 225(2), 209–219. <https://doi.org/10.1111/joa.12200>
- Gröning, F., Fagan, M., & O'Higgins, P. (2012). Modeling the human mandible under masticatory loads: Which input variables are important? *The Anatomical Record*, 295, 853–863. <https://doi.org/10.1002/ar.22455>
- Grosse, I. R., Dumont, E. R., Coletta, C., & Tolleson, A. (2007). Techniques for modeling muscle-induced forces in finite element models of skeletal structures. *Anatomical Record*, 290(9), 1069–1088. <https://doi.org/10.1002/ar.20568>
- Grubich, J. R., Huskey, S., Crofts, S., Orti, G., & Porto, J. (2012). Mega-Bites: Extreme jaw forces of living and extinct piranhas (Serrasalminae). *Scientific Reports*, 2(1). <https://doi.org/10.1038/srep01009>
- Geuzaine, C., & Remacle, J.-F. (2009). Gmsh: a three-dimensional finite element mesh generator with built-in pre- and post-processing facilities. *International Journal for Numerical Methods in Engineering*, 79(11), 1309–1331.
- Huiskes, R., & Hollister, S. J. (1993). From structure to process, from organ to cell: Recent developments of FE-analysis in orthopaedic biomechanics. *Journal of Biomechanical Engineering*, 115, 520–527.
- Joshi, J., Manral, A. R., Maurya, S., & Vishnoi, M. (2021). Biomechanical analysis of human tibia bone based on FEA. *Materials Today: Proceedings*, 44, 1711–1717. <https://doi.org/10.1016/J.MATPR.2020.11.877>
- Krings, W., Marcé-Nogué, J., Karabacak, H., Glaubrecht, M., & Gorb, S. N. (2020). Finite element analysis of individual taenioglossan radular teeth (Mollusca). *Acta Biomaterialia*, 115, 317–332. <https://doi.org/10.1016/J.ACTBIO.2020.08.034>
- Laurent, C. P., Böhme, B., Mengoni, M., D'Ottreppe, V., Balligand, M., & Ponthot, J. P. (2016). Prediction of the mechanical response of canine humerus to three-point bending using subject-specific finite element modelling. *Proceedings of the Institution of Mechanical Engineers, Part H: Journal of Engineering in Medicine*, 230(7), 639–649. <https://doi.org/10.1177/0954411916644269>
- Laurent, C. P., Böhme, B., Verwaerde, J., Papeleux, L., Ponthot, J.-P., & Balligand, M. (2020). Effect of orthopedic implants on canine long bone compression stiffness: A combined experimental and computational approach. *Proceedings of the Institution of Mechanical Engineers, Part H: Journal of Engineering in Medicine*, 234(3), 255–264. <https://doi.org/10.1177/0954411919882603>
- MacLaren, J. A., & Nauwelaerts, S. (2016). A three-dimensional morphometric analysis of upper forelimb morphology in the enigmatic tapir (*Perissodactyla: Tapirus*) hints at subtle variations in locomotor ecology. *Journal of Morphology*, 277(11), 1469–1485. <https://doi.org/10.1002/jmor.20588>
- Matthews, F. L., & West, J. B. (1972). Finite element displacement analysis of a lung. *Journal of Biomechanics*, 5(6), 591–600. [https://doi.org/10.1016/0021-9290\(72\)90031-0](https://doi.org/10.1016/0021-9290(72)90031-0)
- Mengoni, M., Ponthot, J. P., & Boman, R. (2016). Mesh management methods in finite element simulations of orthodontic tooth movement. *Medical Engineering and Physics*, 38(2), 140–147. <https://doi.org/10.1016/j.medengphy.2015.11.005>
- Morales-García, N. M., Burgess, T. D., Hill, J. J., Gill, P. G., & Rayfield, E. J. (2019). The use of extruded finite-element models as a novel alternative to tomography-based models: A case study using early mammal jaws. *Journal of the Royal Society Interface*, 16(161), 20190674. <https://doi.org/10.1098/rsif.2019.0674>
- Porro, L. B., Holliday, C. M., Anapol, F., Ontiveros, L. C., Ontiveros, L. T., & Ross, C. F. (2011). Free body analysis, beam mechanics, and finite element modeling of the mandible of Alligator mississippiensis. *Journal of Morphology*, 272(8), 910–937. <https://doi.org/10.1002/jmor.10957>
- Porro, L. B., Metzger, K. A., Iriarte-Diaz, J., & Ross, C. F. (2013). In vivo bone strain and finite element modeling of the mandible of Alligator mississippiensis. *Journal of Anatomy*, 223(3), 195–227. <https://doi.org/10.1111/joa.12080>
- Püschel, T. A., Marcé-Nogué, J., Gladman, J. T., Bobe, R. R., & Sellers, W. I. (2018). Inferring locomotor behaviours in Miocene New World monkeys using finite element analysis, geometric morphometrics and machine-learning classification techniques applied to talar morphology. *Journal of the Royal Society Interface*, 15(146), 20180520. <https://doi.org/10.1098/rsif.2018.0520>
- Rayfield, E. J., Norman, D. B., Horner, C. C., Horner, J. R., Smith, P. M., Thomason, J. J., & Upchurch, P. (2001). Cranial design and function in a large theropod dinosaur. *Nature*, 409(6823), 1033–1037. <https://doi.org/10.1038/35059070>
- Rybicki, E. F., Simonen, F. A., & Weis, E. B. (1972). On the mathematical analysis of stress in the human femur. *Journal of Biomechanics*, 5(2), 203–215. [https://doi.org/10.1016/0021-9290\(72\)90056-5](https://doi.org/10.1016/0021-9290(72)90056-5)
- Smith, J. M., & Cohen, R. J. (1984). Simple finite-element model accounts for wide range of cardiac dysrhythmias. *Proceedings of the National Academy of Sciences of the United States of America*, 81(11), 233–237. <https://doi.org/10.1073/pnas.81.1.233>
- Tseng, Z. J. (2009). Cranial function in a late Miocene *Dinocrocota gigantea* (Mammalia: Carnivora) revealed by comparative finite element analysis. *Biological Journal of the Linnean Society*, 96(1), 51–67. <https://doi.org/10.1111/j.1095-8312.2008.01095.x>
- Wroe, S., Huber, D. R., Lowry, M., McHenry, C., Moreno, K., Clausen, P., Ferrara, T. L., Cunningham, E., Dean, M. N., & Summers, A. P.

- (2008). Three-dimensional computer analysis of white shark jaw mechanics: How hard can a great white bite? *Journal of Zoology*, 276(4), 336–342. <https://doi.org/10.1111/j.1469-7998.2008.00494.x>
- Zapata, U., Metzger, K., Wang, Q., Elsey, R. M., Ross, C. F., & Dechow, P. C. (2010). Material properties of mandibular cortical bone in the American alligator. *Alligator mississippiensis. Bone*, 46(3), 860–867. <https://doi.org/10.1016/j.bone.2009.11.010>
- Zhou, Z., Winkler, D. E., Fortuny, J., Kaiser, T. M., & Marcé-Nogué, J. (2019). Why ruminating ungulates chew sloppily: Biomechanics discern a phylogenetic pattern. *PLoS ONE*, 14(4), e0214510. <https://doi.org/10.1371/JOURNAL.PONE.0214510>
- Zienkiewicz, O. C., & Morice, P. B. (1971). *The finite element method in engineering science* (2nd ed.). McGraw-Hill.
- Zienkiewicz, O. C., Taylor, R. L., & Zhu, J. Z. (2005). *Finite element method for solid and structural mechanics* (6th ed.). Elsevier Butterworth-Heinemann.

SUPPORTING INFORMATION

Additional supporting information can be found online in the Supporting Information section at the end of this article.

Data S1 Fossils: a new, fast, and open-source protocol to simulate muscle-driven biomechanical loading of curved bone.

How to cite this article: Chatar, N., Boman, R., Fallon Gaudichon, V., MacLaren, J. A., & Fischer, V. (2022). 'Fossils': A new, fast and open-source protocol to simulate muscle-driven biomechanical loading of bone. *Methods in Ecology and Evolution*, 00, 1–12. <https://doi.org/10.1111/2041-210X.14051>